Global Change Biology

WILEY

Global Change Biology

RESEARCH ARTICLE

Apex Scavenger Declines Have Cascading Effects on Soil Biogeochemistry and Ecosystem Processes

Torrey Stephenson[1] | David W. Crowder[2] | Ernest Osburn[3] | Michael Strickland[1] | Menna Jones[4] | Savannah Bartel[2] | Kawinwit Kittipalawattanapol[4] | Calum X. Cunningham[4] | Tara Hudiburg[5] | Andrew Storfer[6] | Julia Piaskowski[1] | Laurel Lynch[1]

[1]College of Agriculture and Life Sciences, University of Idaho, Moscow, Idaho, USA | [2]Department of Entomology, Washington State University, Pullman, WA, USA | [3]Department of Plant and Soil Sciences, University of Kentucky, Lexington, Kentucky, USA | [4]School of Natural Sciences, University of Tasmania, Hobart, Tasmania, Australia | [5]College of Natural Resources, University of Idaho, Moscow, Idaho, USA | [6]School of Biological Sciences, Washington State University, Pullman, WA, USA

Correspondence: Torrey Stephenson (torreys@uidaho.edu)

Received: 22 May 2025 | **Revised:** 1 September 2025 | **Accepted:** 4 September 2025

Funding: This work was supported by National Science Foundation, DEB-2054716.

Keywords: carbon cycling | microbial ecology | nutrient cycling | scavengers | soil biogeochemistry | trophic downgrading

ABSTRACT

Global apex scavenger declines strongly alter food web dynamics, but studies rarely test whether trophic downgrading impacts ecosystem functions. Here, we leverage a unique, disease-induced gradient in Tasmanian devil (*Sarcophilus harrisii*) population densities to assess feedbacks between carcass persistence, subordinate scavenger guilds, and biogeochemical cycling. We further explored interkingdom and seasonal interactions by manipulating carcass access and replicating experiments in warmer, drier summer versus cooler, wetter winter periods. We show Tasmanian devil declines significantly extend carcass persistence and increase the flux of carcass-derived nutrients belowground (e.g., by 18–134-fold for ammonium). Greater nutrient availability reduces soil microbiome diversity by up to 26%, increasing the relative abundance of putative zoonotic pathogens. Nutrient subsidies also shift microbial communities toward faster-growing taxa that invest less energy in resource acquisition, with implications for soil carbon sequestration. Rates of carcass decomposition were reduced in the winter, dampening soil biogeochemical responses and interkingdom competition. Notably, while less efficient scavenger guilds clearly facilitate carcass consumption, they were not able to fill the functional role of apex scavengers. Our study illustrates how trophic downgrading effects can ripple across all levels of ecological organization.

1 | Introduction

The decomposition of animal inputs transfers ~2 billion metric tons of biomass into the global dead organic matter pool annually (Bar-On et al. 2018). As this is far less than the ~320 billion metric tons provided by plants (Bar-On et al. 2018), animal inputs are often disregarded in the context of soil biogeochemistry. However, animal inputs are enriched in macro- and micronutrients that govern biological functions, such as metabolism and enzyme synthesis, and are relatively rare in the soil ecosystem (Benbow et al. 2019; DeBruyn et al. 2024). Indeed, higher quality carrion with lower carbon:nitrogen ratios decomposes more rapidly than lower quality plant inputs, creating biogeochemical "hotspots" that impact rates of carbon, nutrient, and trace element cycling (Carter et al. 2006; Keenan et al. 2018). Carrion resources can also be spread across landscapes by diverse communities of scavengers that include vertebrates, invertebrates, and microorganisms (Bartel et al. 2024).

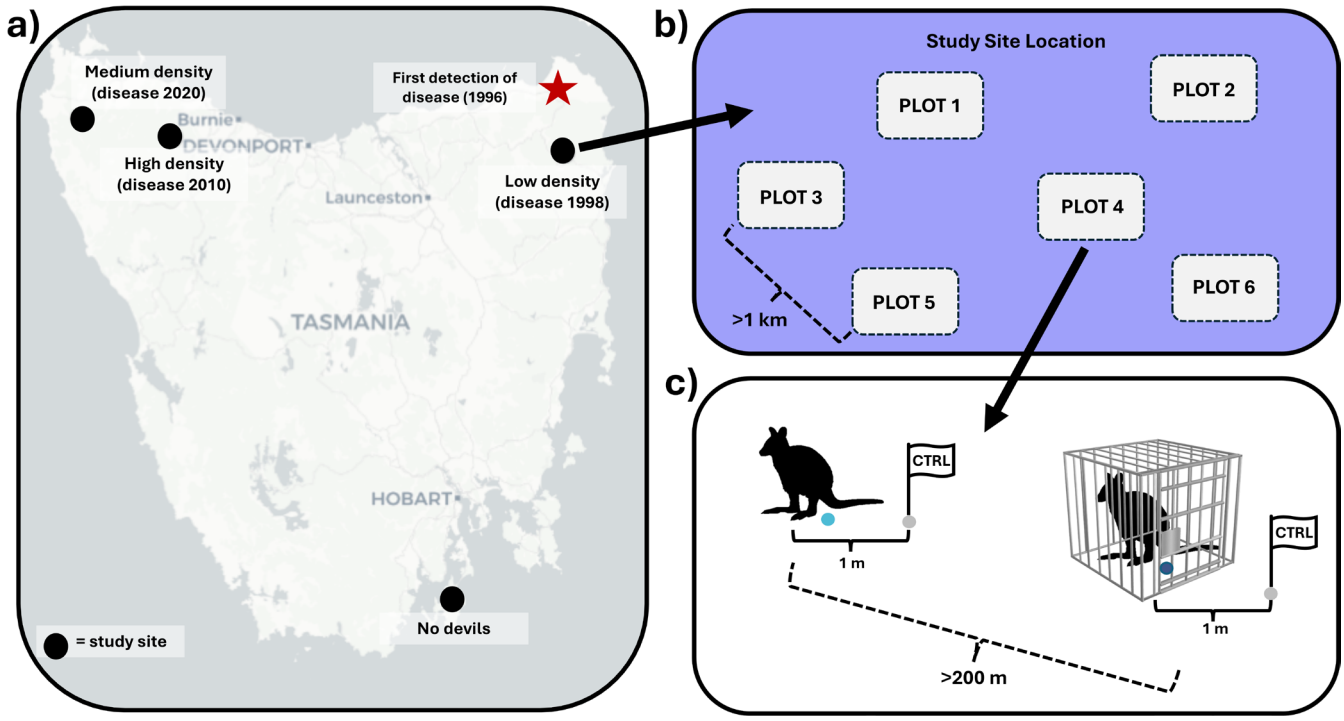

FIGURE 1 | Map of Tasmania, Australia showing (a) field sites spanning the devil decline gradient (circles) with the approximate year of devil facial tumor disease arrival, along with the first detected location of devil facial tumor disease (star), (b) representation of experimental plot layout at each site ($n = 6$), separated by at least 1 km, and (c) detailed representation of plot layout including both open and caged carcasses separated by at least 200 m, as well as paired control sample sites located 1 m from each carcass. Dots in panel (c) represent locations where soil samples were collected at 0, 5, 10, 15, and 30 days after carcass placement. Map lines delineate study areas and do not necessarily depict accepted national boundaries.

Interkingdom interactions among scavenger guilds mediate carcass decomposition (Cunningham et al. 2018). Although vertebrate scavengers can broadly disperse nutrients across landscapes, microorganisms break down carcasses locally, concentrating nutrients to form "cadaver decomposition islands" (Carter et al. 2006). These nutrient pulses move laterally and vertically into the soil profile, altering soil biogeochemical properties and potentially selecting for microbial taxa that are able to rapidly assimilate ephemeral resources ("copiotrophs;" Burcham et al. 2024). Complicating these interkingdom feedbacks, invertebrate scavengers, such as blowflies, drawn to carrion by volatile compounds released during bacterial decomposition, can inoculate carcasses with novel microorganisms (Metcalf et al. 2016); yeasts and bacteria can similarly be transmitted to carcasses via anal secretions of necrophagous burying beetles (Vogel et al. 2017). As unique scavenger species vary widely in their ability to assimilate and distribute carrion-derived resources, shifts in scavenger community composition can impact spatiotemporal patterns in carrion decomposition and alter broader ecosystem functions (Bartel et al. 2024; DeBruyn et al. 2024; Stephenson et al. 2024).

Globally, population declines of apex species have resulted in trophic downgrading (Estes et al. 2011; Ordiz et al. 2021; Ripple et al. 2014, 2017), causing less-efficient subordinate scavengers to compete for carcass resources. For instance, Tasmanian devils (*Sarcophilus harrisii* , hereafter 'devils') are the dominant scavenger on the Australian island of Tasmania and one of only three "true bone eaters" (or osteophages) globally, with exceptionally strong bite forces that allow them to rapidly consume carcasses and bone material (Jones 1997). However, in several areas of Tasmania, devil populations have been dramatically reduced by a lethal transmissible facial cancer, devil facial tumor disease, relaxing interference competition for foraging by other species (Cunningham et al. 2018). Devil facial tumor disease was first discovered in northeastern Tasmania in 1996 and has spread westward, reducing devil populations by at least 68%, with the greatest declines observed within 10 years of disease arrival (Cunningham et al. 2021; Hawkins et al. 2006; Woods et al. 2018). This natural population density gradient makes Tasmania ideal for testing impacts of trophic downgrading on soil processes, as devil declines are occurring independent of human conflict or land-use change.

Here, we examined whether disease-induced declines in devil population densities have cascading effects on soil microbiomes and, consequently, ecosystem function. We established experiments at four sites spanning the devil density gradient to test whether altered scavenger communities affected decomposition, soil microbiomes, and biogeochemical cycles (Figure 1). At each site, we manipulated apex scavenger access (open versus caged carcasses to exclude foraging by adult devils) and repeated our experiment in winter and summer. We predicted that carcasses would persist longer at low devil density sites and where adult devils were excluded, increasing the flow of carcass-derived nutrients into the soil. We also expected these nutrient-rich subsidies would select for copiotrophic microorganisms that capitalize on pulsed resources and allocate less energy toward extracellular enzyme production, increasing the proportion of carbon respired versus sequestered belowground

(Ma et al. 2023). Finally, we predicted devil density and access would shape soil microbial community composition and function more in the summer than in winter, reflecting greater biological activity of invertebrate and microbial consumers.

2 | Materials and Methods

2.1 | Study Sites and Data Collection

Our study was conducted at four sites with variable devil population density, which was related but not perfectly correlated to the time since first arrival of devil facial tumor disease.

For example, total devil densities were higher at the central than western site, despite initial disease transmission from east to west, likely driven by rapid host-tumor coevolution (Clement et al. 2025) and genome evolution (Epstein et al. 2016; Margres et al. 2020) at the central site (Figure 1). At the time of our experiment (2022 and 2023), predicted devil densities per km were: (i) low devil density (Blue Tier, disease detected in 1998, 0.12 ± 0.01), (ii) medium devil density (Salmon River, disease detected in 2020, 0.26 ± 0.01), (iii) high devil density (West Takone, disease detected in 2010, 0.42 ± 0.05), and a (iv) no devil control (Bruny Island, no recent history of devils, 0.0 ± 0.0; Cunningham et al. 2021). Estimated devil population densities at each site are fairly robust, as adult devils have relatively stable home ranges (~4.5 km diameter; Pemberton 1990). Visitation by the same individual to multiple sites was unlikely, given that home ranges are about an order of magnitude smaller than the distance between sites (≥ 50 km) and that the maximum recorded daily movement distance for adult devils is less than half the distance separating any two sites (Andersen et al. 2017). Finally, we selected the four focal study sites to be located in wet eucalyptus forest at similar elevation, thus minimizing differences in habitat, climate, and soil properties (Table S1).

Our field sites captured a natural gradient in devil density (Cunningham et al. 2021), but to further assess the effects of devils on soil biogeochemical processes, we conducted a manipulative experiment at each site where we deployed animal carcasses available to all scavengers (hereafter "open", $n = 6$ per site) or caged to prevent carcass use by adult devils (hereafter "excluded", $n = 6$ per site). The experiments at each site were arranged as a split-plot design with carcass access (excluded, open) as the main plot and location (carcass treatment, paired control) as the split plot. For both open and excluded treatments, we used Tasmanian pademelon (*Thylogale billardierii*) carcasses as our experimental unit (mean weight 4.8 kg), as they are a common prey animal in Tasmania that account for a substantial portion of devil and other subordinate scavengers' diets (Andersen et al. 2017; Fancourt 2015; Pemberton et al. 2008). Pademelon carcasses were obtained from licensed local game meat suppliers; all animals were killed with a single headshot to preserve tissue integrity. All carcasses were secured to the ground using small star pickets (45 cm). Pickets were driven into the soil (~20 cm deep) through the chest cavity to prevent carcass relocation by scavengers, enabling repeated sampling and game camera imaging at treatment sites. Securing carcasses with a star picket may have produced an upper estimate of belowground nutrient delivery by limiting the dispersal of carcass remains by scavengers. However, previous work indicates that adult devils predominantly engage in bouts of "gorge feeding" (Pemberton and Renouf 1993), rapidly consuming carcasses at a single location. Consequently, we expect our findings to reflect realistic decomposition dynamics under natural conditions. Excluded carcasses were further placed within weld-mesh cages ($110 \times 168 \times 100$ cm with 12×12 cm openings) that excluded adult devils, though not other smaller scavengers. Excluded and open carcasses were spaced at least 200 m apart, and replicates were separated by ~1 km to minimize visitation to multiple carcasses by the same animal. We recorded carcass visitation using remote game cameras (Swift Enduro) strapped to a tree ~1 m above ground and ~0.6 m from the carcass. Experiments were established for 24–30 days to capture carcass decomposition dynamics in winter (August to September 2022) and summer (February to March 2023; Table S1). Some treatments were compromised (e.g., weather, cage failures, etc.), resulting in unequal sample sizes, which were accounted for in statistical models (Table S1 presents actual sample numbers).

In winter, we collected soil samples the day of carcass deployment (day 0) and at the end of the experiment (day 24); during summer, we collected soil samples 0, 5, 10, 15, and 30 days after carcass deployment to capture temporal dynamics. Samples were collected from the top 7 cm of soil after removing any litter. Treatment samples were collected under the carcass, and control samples were collected ~1 m away to account for background temporal changes in microbial or soil biogeochemical properties. We used a 4 cm sterilized soil corer to collect samples, which were homogenized by hand before dividing them into two subsamples. The first subsample was used for biochemical analysis, was initially placed on ice, and then stored at −20°C within 48 h of collection. The second subsample was used for moisture and geochemical analyses and was oven-dried at 60°C, sieved to 2 mm, and stored at ambient temperature. All samples were then shipped to the University of Idaho following USDA import permits and using a courier service (LabCabs Australia) to ensure they remained frozen if necessary during transport.

We recorded carcass consumption and generated total consumption scores by estimating percent consumption of five predetermined tissue types. Values for each type were weighted to represent their contribution to total carcass mass: (i) organs: 30%, (ii) muscles: 35%, (iii) bones: 25%, (iv) tail: 5%, and (v) hide: 5% (Sterner and Elser 2002). The variable 'carcass persistence' is the total number of days that any soft tissue remained, using total consumption observations at each sampling period and game camera photos for making these determinations (Figures S9 and S10).

2.2 | Abiotic Data

HOBO pendant temperature data loggers (Onset Computer Corporation) were deployed at each carcass to record ambient temperatures at 15-min intervals for all trials. Temperature data were downloaded from intact loggers at the conclusion of the experiment and averaged to obtain mean daily air temperature at each site. We calculated accumulated degree days by summing the daily mean temperatures over 0°C from the time of carcass deployment (Burcham et al. 2024; Strickland et al. 2015). We

obtained daily precipitation measurements from the Australian Bureau of Meteorology, using the weather station closest to each study site.

2.3 | Soil Assays

We obtained soil gravimetric water content by dividing the difference in mass between samples before and after drying at 60°C for 48 h by the final dry mass of soil. We determined pH and electrical conductivity on a 1:5 slurry (2 mm dried soil:DI water) that had equilibrated for 15 min (Jenway 3540 Bench Combined Conductivity/pH Meter, calibrated daily).

We determined soil C, N, P, Ca, Fe, and Al concentrations on finely ground subsamples homogenized with a Mini-BeadBeater 96 (Biospec Products). Soil C and N were quantified at the Washington State University Stable Isotope Core Laboratory with an elemental analyzer (ECS 4010; Costech). We determined P, Ca, Fe, and Al content by dry ashing 0.5 g of ground soil in a furnace at 500°C for 3 h, then digesting samples with a stepwise addition of 2:1:2 parts nitric acid, hydrogen peroxide, and hydrochloric acid (US EPA, Method 3050B, 2019) prior to ICP-OES analysis (Agilent 5110). A reference sample of San Joaqin Soil (SRM 2709a) was included in each batch run to determine digestion recovery efficiencies.

We quantified extractable pools of dissolved organic carbon and total dissolved nitrogen as well as inorganic nutrients, nitrate (NO_3-N) and ammonium (NH_4-N), for each sample. Briefly, we extracted 10 g of thawed soil with 50 mL of a 0.05 M K_2SO_4 solution, mixed slurries at 200 rpm for 1 h on an orbital shaker table, and then filtered extracts with Whatman #1 paper. Total dissolved organic carbon and total dissolved nitrogen were assessed using a TOC-L autoanalyzer (Shimadzu Scientific Instruments Inc.); organic nitrogen is the sum of ammonium and nitrate subtracted from total dissolved nitrogen. Inorganic nutrients were determined using colorimetric analyses on a Spectramax M2 spectrophotometer (Molecular Devices), with NO_3-N quantified using the vanadium (III) chloride method (Doane and Horwáth 2003), and NH_4-N with the phenol-hypochlorite method (Weatherburn 1967). Despite repeated dilution and centrifugation, the high organic content of some extracts interfered with the colorimetric analysis of phosphate (PO_4-P), and we were unable to include analysis of this inorganic nutrient in our study.

2.4 | Microbial Analyses

We extracted DNA from 0.5 g of thawed soil using a PowerSoil Pro Kit (Qiagen, Valencia, CA, US), and diluted extracts 10-fold prior to PCR amplification of bacterial and fungal marker regions. We used primer pair 515F/806R to target the V4 region of the 16S rRNA gene for (Walters et al. 2016) and ITS1f/ITS2r primers to target the fungal ITS1 region (White et al. 1990); PCR amplification was confirmed using gel electrophoresis and PCR products were quantified on a Qubit Fluorometer (ThermoFisher Scientific, Waltham, MA, US). PCR products were pooled in equimolar ratios and the pooled libraries purified using the Qiaquick PCR purification kit. Purified amplicon libraries were sequenced at the Duke University GCB Sequencing and Genomic Technologies Shared Resource using an Illumina MiSeq with 250-bp paired-end reads. Raw reads were deposited in the NCBI archive under accession number PRJNA1238269.

We processed demultiplexed sequencing data using the "DADA2" package in R (Callahan et al. 2016). Version 4.3 (R Core Team 2024) of R was used for all data preparation and analytical steps that required the software. Sequence reads were trimmed and filtered using the following parameters: truncLen = c(200,150); maxN = 0; maxEE = c(2,2); truncQ = 2. Reads were then dereplicated, processed, forward and reverse reads were merged, and chimeras were removed. Next, we assigned taxonomy using the IDTAXA algorithm (from the "decipher" package; Wright 2016), referencing the SILVA database version 138 for 16S (Quast et al. 2013) and the UNITE database version 8.3 for ITS (Abarenkov et al. 2010). After constructing phyloseq objects (R package "Phyloseq;" McMurdie and Holmes 2013), we removed samples with sequence depths < 10,000 reads, including the method blank for each run ($n = 10$ for 16S; $n = 1$ for ITS). We filtered out eukaryotes from the 16S dataset and amplicon sequence variants (ASVs) that were not classified at the kingdom level, then rarefied sequences to equalize the number of reads across samples (10,001 sequences for 16S; 21,557 sequences for ITS).

To identify fungal taxa driving potential shifts in community function, we assigned functional information to ITS ASVs using the R package "FunGuild" (Nguyen et al. 2016) and examined the relative abundance of trophic modes (e.g., saprotroph, symbiotroph, pathotroph, and their combinations) across seasons, sites, and treatments. Combinations of modes indicate fungi with facultative trophic strategies that may be dependent on environmental conditions or life stage; understanding shifts in dominant trophic modes provides insight into how scavenger-mediated nutrient inputs shape fungal community structure and ecosystem processes.

We assessed bacterial growth potential, or copiotrophic versus oligotrophic life strategies, by using PICRUSt2 (Douglas et al. 2020) with default parameters to estimate 16S copy numbers for each sequence and then calculating treatment-level relative abundance weighted averages for each site, time, and treatment combination. We also used PICRUSt2 to identify the predicted relative abundances of metabolic pathways including ornithine and lysine decarboxylase, and genes encoding extracellular enzymes targeting C, N, and P (Table S2). We further assessed the relative abundance of bacteria classified as putative copiotrophs (Proteobacteriota, Firmicutes, Bacteroidota) versus oligotrophs (Verrucomicrobiota, Acidobacteriota) for each sample (Fierer et al. 2007).

We quantified counts of bacterial genera associated with necrophagous flies (*Ignatzschineria*, *Morganella*, *Providencia*, and *Wohlfahrtiimonas*) from sequencing data; these genera also commonly contain pathogenic species and strains (Gold et al. 2020; Gupta et al. 2011; Lee et al. 2014). To further identify potential human pathogens in control and carcass-impacted soils, nucleotide sequences were aligned against a bacterial pathogen 16S sequence database using the Basic

Local Alignment Search Tool (BLAST; Altschul et al. 1990). Using "makeblastdb" (BLAST+ v2.16.0), we created a custom database of pathogen 16S rRNA gene sequences from the multiple bacterial pathogen detection database using default parameters (Yang et al. 2023), and aligned our ASV sequences to the database to identify and quantify putative human pathogens. Alignments were filtered based on percent identity (> 97%) and an e value of $< 1e^{-5}$ to ensure high-quality matches; then read counts of putative pathogens were summed for each sample.

Finally, we visualized microbial families that were unique or common across treatments using UpSet plots (R package "ComplexUpset;" Krassowski et al. 2022). Briefly, for both ITS and 16S ASVs, we generated plot data by transforming raw reads from the rarefied phyloseq object to relative abundance data, which were aggregated at the family level. We then converted the resulting ASV abundance data to binary presence/absence, then split the data by scavenger access treatment. For plotting purposes, we designated phyla that occurred fewer than eight times in each subdivided dataset as "rare." We then generated UpSet plots to identify common and rare microbial families at control versus carcass locations.

2.5 | Statistical Analyses

We analyzed the summer trial results using a linear mixed model to assess effects of time, location (soil under carcasses or paired controls), adult devil access (excluded vs. open), and all interactions on response variables of (i) carcass persistence, (ii) soil nutrients (total carbon and nitrogen, ammonium, nitrate), (iii) soil pH, and (iv) electrical conductivity at each site separately. Models were fit with the R package "nlme," where time, location, and devil access were fixed effects, and replicate was a random effect nested within the devil access treatment (Equation 1):

$$Y_{ijkl} = \mu + \alpha_i + \beta_j + \gamma_k + (\alpha\beta)_{ij} + (\alpha\gamma)_{ik} + (\beta\gamma)_{jk} + (\alpha\beta\gamma)_{ijk} + r_l + \epsilon^W_{i(l)} + \epsilon^S_{jk(il)} \quad (1)$$

where μ is the overall mean; α_i is the ith location; β_j is the jth devil access; γ_k is the kth time point; r_l is the lth replicate; $\epsilon^W_{i(l)}$ is the main plot error; and $\epsilon^S_{jk(il)}$ is split plot error term. The two-way interactions included are location × access ($\alpha\beta$); location × time ($\alpha\gamma$); and access × time ($\beta\gamma$); the three-way interaction included is location × access × time ($\alpha\beta\gamma$). We accounted for correlations over time using a lag1 autoregressive (AR1) correlation structure. Model fit was assessed by manually inspecting residual-versus-fitted values and qq-plots. For the proportion variables (carcass consumption and relative abundance of microbial taxa), a generalized linear mixed model with the beta distribution and logit link function was used, following the same model specification described above. Model fit was assessed with the package "DHARMa" (Hartig 2022). Marginal means and standard errors for treatment effects were obtained from all models with R package "emmeans" (Lenth 2024).

The overall impacts of site-by-time, site-by-devil access, and site-by-location were assessed for all dependent variables using a linear model and generalized least squares (R package "nlme;" Equation 2).

$$Y_{ijkl} = \mu + \alpha_i + \beta_j + \gamma_k + \delta_l + r_m + \epsilon^W_{i(m)} + \epsilon^S_{jk(im)} \quad (2)$$

where μ is the overall mean; α_i is the ith location; β_j is the jth devil access; γ_k is the kth time point; δ_l is the lth field site; r_m is the mth replicate; $\epsilon^W_{i(l)}$ is the main plot error; and $\epsilon^S_{jk(il)}$ is split plot error term. All interactions were included in the final model but are not shown in Equation (2) for simplicity. This model was fit in two stages: first, marginal means for location-by-devil access-by-time effects from the previous analyses were estimated. Those estimates were used for model fitting in the second stage, weighting each by the inverse of its standard error. As before, we handled the repeated measures component "time" by using an AR1 correlation structure; model diagnostics were visually checked by examining residual plots, and marginal means were estimated using "emmeans." GLMMs were likewise fit in a two-stage procedure for the proportion data. Pairwise comparisons exploring interaction terms were adjusted using the false discovery rate.

The impact of seasonal variation (winter versus summer) was examined by fitting a mixed model to evaluate the effects of season, location, devil access, and site on all dependent variables at the final time point (Equation 3):

$$Y_{ijkl} = \mu + \alpha_i + \beta_j + \gamma_k + \delta_l + (\alpha\beta)_{ij} + (\alpha\gamma)_{ik} + (\beta\gamma)_{jk} + (\alpha\beta\gamma)_{ijk} + r_m + \epsilon^W_{i(m)} + \epsilon^S_{jk(im)} \quad (3)$$

where μ is the overall mean; α_i is the ith location; β_j is the jth devil access; γ_k is the kth season; δ_l is the lth field site; r_m is the mth replicate; $\epsilon^W_{i(l)}$ is the main plot error; and $\epsilon^S_{jk(il)}$ is split plot error term. All interactions (location × access ($\alpha\beta$), location × time ($\alpha\gamma$), access × time ($\beta\gamma$), and location × access × time ($\alpha\beta\gamma$)) were included in the final model. All variables except replicate were fixed effects and replicate (nested within site) was a random effect. As described previously, a generalized linear model was used for all proportion variables (with a beta distribution and logit link function) and a general linear model was used for the remaining dependent variables.

We calculated microbial α-diversity using Shannon and Simpson diversity indices, and visualized changes in α-diversity between adult devil access (open vs. excluded) and location (paired carcass and control) using heat maps. We calculated the Bray–Curtis dissimilarity matrix and performed permutational multivariate analysis of variance to test for treatment-based differences in community composition, and assessed differences in bacterial β-diversity using the "betadisper" function in the R package "vegan" (Oksanen et al. 2001). We tested for differentially abundant bacterial phyla from days 5 through 15 using ALDEx2 (Gloor et al. 2016), applying 128 Monte Carlo Dirichlet instances to generate robust estimates of centered log-ratio-transformed abundances. Analyses were conducted on unrarefied sequence data agglomerated at the phylum level. First, we subset data by site and tested for treatment effects (Control, Open, and Excluded) within each site. Next, we subset data by carcass access (Open vs. Excluded) and tested for differentially abundant phyla across sites,

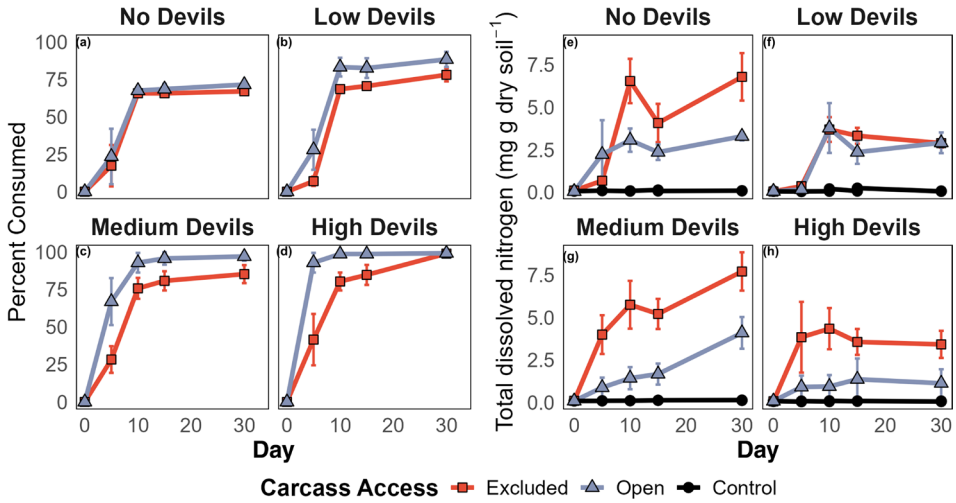

FIGURE 2 | (a–d) Total consumption of pademelon carcasses and (e–h) total dissolved nitrogen concentrations at each site in the summer trial; similar trends were observed for other biogeochemical parameters (see Tables S3–S9). Panels represent sites spanning the gradient of devil density and symbols reflect carcass access. Standard error bars reflect variability across replicates ($n = 6$ per treatment).

excluding the No-Devil control site. We assessed pathogen abundance between carcass and control soil samples across all sites and times using a Wilcoxon rank sum test with a continuity correction.

3 | Results

3.1 | Carcass Consumption

We first tested how adult devil access affected carcass consumption across sites that varied in devil density (Figure 1). Because carcass consumption rates and soil biogeochemical responses were more dynamic in the summer, we focus on summer results and present winter dynamics primarily for comparison. Across all sites, consumption was lower at excluded than open carcasses by day 30 (89 ± 6.3 vs. 82% ± 6.7%) ($\chi^2 = 7.66$, $p < 0.01$; Figure 2a; Figure S1). These differences were driven by high and medium devil density sites, especially at early time points; at the no devil site, total carcass consumption did not differ between open and excluded carcasses until day 30 (72 ± 1.5 vs. 67% ± 1.5%; Figure 2a; Figure S1). Bone consumption was also greater at open (79.4% ± 7.86%) than excluded (50.6% ± 9.76%) carcasses ($F_{1,33} = 10.0$; $p < 0.01$). Consumption differed across sites ($\chi^2 = 11.4$, $p < 0.01$); it was highest at the high devil density site (99% ± 0.1%) followed by the medium devil density site (91% ± 5.9%), the low devil density site (83% ± 5.2%), then the no devil site (69% ± 2.3%). Accumulated degree days were 51%–65% lower in the winter, and precipitation was on average 125% higher (Table S1), which facilitated more complete and rapid carcass consumption in summer (88.1% ± 2.4%) than winter (62.5% ± 6.7%) ($\chi^2 = 10.8$, $p < 0.01$). Carcass soft tissues also persisted for significantly less time in summer (10.4 ± 1.2 days) than in winter (17.1 ± 1.4 days) ($\chi^2 = 4.7$, $p < 0.05$; Tables S2–S9; Figure S1). Regardless of adult devil scavenger access, bone removal in the summer was significantly higher at the high and medium devil density sites (~75% ± 10.5% and 98% ± 1.2%) than at the low density and no devil sites (46% ± 12.4% and 5% ± 3.2%) ($\chi^2 = 22.9$, $p < 0.001$).

3.2 | Soil Biogeochemistry

Soil nitrogen levels increased faster under carcasses than paired controls, although the timing and magnitude of nitrogen inputs varied by adult devil access and across the devil density gradient (Figure 2b). Total dissolved nitrogen was up to fivefold higher at excluded than open carcasses, with significant differences first detected at the medium devil density site (Day 5), then the high and low devil density sites (Day 10), and last at the no devil site (Day 15) ($p < 0.05$). At sites with devils, total dissolved nitrogen increased by 10- to 96-fold under excluded carcasses in the first 5 days, with similar but lower magnitude increases detected at open carcasses. At the no devil site, increases in total dissolved nitrogen under carcasses were variable over time, although similar in magnitude to other sites (7- to 105-fold; $F_{4,23} = 15.9$; $p < 0.001$). Ammonium accounted for 41%–99% of total inorganic nitrogen across all sites (Tables S2–S9), and soil ammonium levels were 18- to 134-fold higher under excluded carcasses than paired controls at all sites and times. However, soil ammonium levels were only elevated under open carcasses after Day 5 at the medium and low devil density sites, and after Day 10 at the high devil density and no devil sites (Tables S2–S9). Nitrate levels also varied by time, site, and adult devil access, although patterns were less distinct than other measures (Tables S2–S9). Organic nitrogen accounted for 16.5% ± 2.1% of total dissolved nitrogen under carcasses and 34.0% ± 2.9% at controls ($F_{3,43} = 9.8$; $p < 0.001$). Changes in dissolved organic carbon were similar in trend to total dissolved nitrogen: levels were higher under carcasses than paired controls, with a generally greater response at excluded carcasses, particularly at sites with devils (Tables S2–S9, Figure S2).

Changes in pH were less persistent than carbon or nitrogen, but were typically higher under carcasses than paired controls, increased more under excluded than open carcasses, and were correlated with the devil density gradient ($F_{3,52} = 73.2$, $p < 0.001$; Table S1). Soil pH was higher in the summer at carcasses and paired controls ($\chi^2 = 27.2$, $p < 0.001$). We also observed significant effects of time ($F_{4,52} = 7.5$, $p < 0.001$) and carcass presence ($F_{1,52} = 19.5$, $p < 0.001$) on electrical conductivity, which

increased from Day 0 to 30 at all sites, and was higher under carcasses than paired controls. Soil nutrients and electrical conductivity were significantly higher under carcasses in the summer than in the winter and at excluded than open carcasses (Figure S2).

3.3 | Soil Microbial Communities

Soil under carcasses had faster-growing bacterial taxa, reduced bacterial α-diversity, higher bacterial β-diversity, and lower relative abundance of fungal ectomycorrhizae than paired controls. Across all sites and times, a core microbiome (i.e., taxa found in all soil samples) captured most detected bacterial (70%–82%) and fungal (65%–75%) families (Figure S3). However, carcasses exerted a filtering effect on the core microbiome, so communities under carcasses (particularly excluded carcasses) hosted fewer unique families. After Day 5, the number of bacterial families found only under carcasses was equal to or less than those unique to paired controls, but these differences were more pronounced under excluded (6%–13% fewer than control) than open carcasses (0%–9% fewer; Figure S3b). Similarly, carcasses had 13% (open) to 25% (excluded) fewer unique fungal families than paired controls by Day 30 (Figure S3a).

Shifts in relative abundance of bacterial phyla were found immediately at the no, medium, and high devil density sites, but not until Day 10 at the low devil density site (Tables S10–S14). Across all sites, the relative abundance of Firmicutes increased dramatically under carcasses (995% ± 267%), but the relative abundance of Acidobacteriota (−27% ± 9%), Actinobacteriota (−7.2% ± 6.5%), and Planctomycetota (−41% ± 6%) decreased (Tables S10–S14). Differential abundance analysis from Days 5 to 15 revealed shifts in the relative abundance of 58 unique bacterial genera between carcass sites (both excluded and open) and their paired controls. Within carcass treatments, more genera shifted underneath excluded ($n = 57$) than open ($n = 37$) locations (Figure 3). Genera within the phyla Proteobacteria, Acidobacteriota, and Actinobacteriota were the most responsive to carcass presence. However, overall changes in these phyla were subtle, likely because some constituent genera increased in abundance while others decreased—for example, within Proteobacteria, 15 genera increased and 11 decreased; within Acidobacteria, eight increased and eight decreased; and within Actinobacteriota, six increased and seven decreased. Two genera varied between sites: the abundance of both *Staphylococcus* and *Acidipila* was higher under carcass than paired control locations at the low devil site, but not the high devil site ($p < 0.05$).

Putatively r-selected phyla (Proteobacteriota, Firmicutes, Bacteroidota) were 5.5-fold more abundant than K-selected phyla (Verrucomicrobiota, Acidobacteriota) under carcasses. This shift toward putatively faster-growing taxa was supported by higher average 16S rRNA gene copy numbers per organism under carcasses (1.51 ± 0.04 vs. 1.32 ± 0.01) at all sites on Day 10 ($\chi^2 = 10.2$, $p < 0.05$, Figure 4). We also observed significant increases in fly-associated bacterial genera relative abundance under carcasses at all sites after 5 days ($p < 0.001$), at No- and Low-Devils sites after 10 days ($p < 0.001$), and at all sites with devils after 15 days ($p < 0.05$); by Day 30, differences were no longer statistically significant (Figure S4).

Initial bacterial communities varied across sites at all sampling times ($F_{3,81} = 3.6$, $p < 0.001$; Figure 3). Bacterial communities were significantly different ($p < 0.05$) in carcass versus paired control soils at all but the high devil density site, which differed between paired controls and excluded, but not open, carcasses. Communities at open versus excluded carcasses were also significantly different at high and medium devil density sites, but not low or no devil density sites. Bacterial α-diversity was lower under carcasses at all sites, but only for certain periods (e.g., between 5 and 15 days; Figure S5). Decreases in bacterial α-diversity were stronger at excluded than open carcasses. Bacterial β-diversity was greater under open carcasses than paired controls at all sites and most times ($p < 0.01$). Finally, we observed a higher abundance of putative bacterial pathogens at excluded (+61%) and open (+28%) carcasses than paired controls ($F_{1,52} = 4.2$; $p < 0.05$); pathogens were also more abundant at the no and low devil density sites than the medium and high devil density sites ($F_{3,52} = 4.9$; $p < 0.01$; Figure 5).

Fungal communities differed significantly among sites prior to carcass placement ($F_{3,81} = 3.6$, $p < 0.001$) and between carcasses and paired control soils by Day 30 ($F_{3,81} = 3.2$; $p < 0.01$; Figure S6b); we observed no differences in fungal communities between open and excluded carcasses. Neither fungal α- nor β-diversity differed for any site or treatment (Figure S7), although carcass presence did impact fungal trophic mode by Day 30 (Figure 5). Specifically, fungi classified as 'pathotroph-saprotroph' were more abundant under open carcasses than controls at the high devil density site, and under excluded than open carcasses or paired controls at the medium devil density site ($\chi^2 = 21.4$, $p < 0.01$). Fungi classified as 'symbiotroph' decreased under excluded and open carcasses compared to paired controls ($\chi^2 = 7.5$, $p < 0.05$), and those classified as 'saprotroph-symbiotroph' were higher under excluded than open carcasses and paired controls ($\chi^2 = 9.7$; $p < 0.01$). The symbiotrophic guild 'ectomycorrhizae' was detected in all samples, but relative to controls (33.6% ± 4.1%) they decreased under excluded (−8.8% ± 2.0%) and open (−14.4% ± 5.1%) carcasses ($F_{3,78} = 6.5$; $p < 0.001$).

We next assessed changes in metabolic pathways associated with tissue decomposition and nutrient acquisition by calculating the predicted relative abundance of genes encoding specific enzymes using the output from PICRUSt2 (Table S15). Specifically, ornithine decarboxylase (Kegg Ortholog K01581), which catalyzes the conversion of ornithine to putrescine, had a significantly higher predicted relative abundance at control than at carcass locations at all sites ($F_{3.52} = 14.3$, $p < 0.001$, Figure 6). Decreases in the predicted relative abundance of ornithine decarboxylase were detected by Day 5 at the high and medium devil density sites, and by Day 10 at the low devil density and no devil sites. Lysine decarboxylase (Kegg Ortholog K01582), which catalyzes the conversion of lysine to cadaverine, did not differ between carcass access treatments ($p = 0.14$). The predicted relative abundances of genes encoding for seven common hydrolytic extracellular enzymes, which drive C, N, and P cycling in soils, were also lower under carcasses than controls ($p < 0.05$). The predicted relative abundance of genes encoding acid phosphatases was also higher under open than under excluded carcasses ($F_{1,52} = 4.20$; $p < 0.05$).

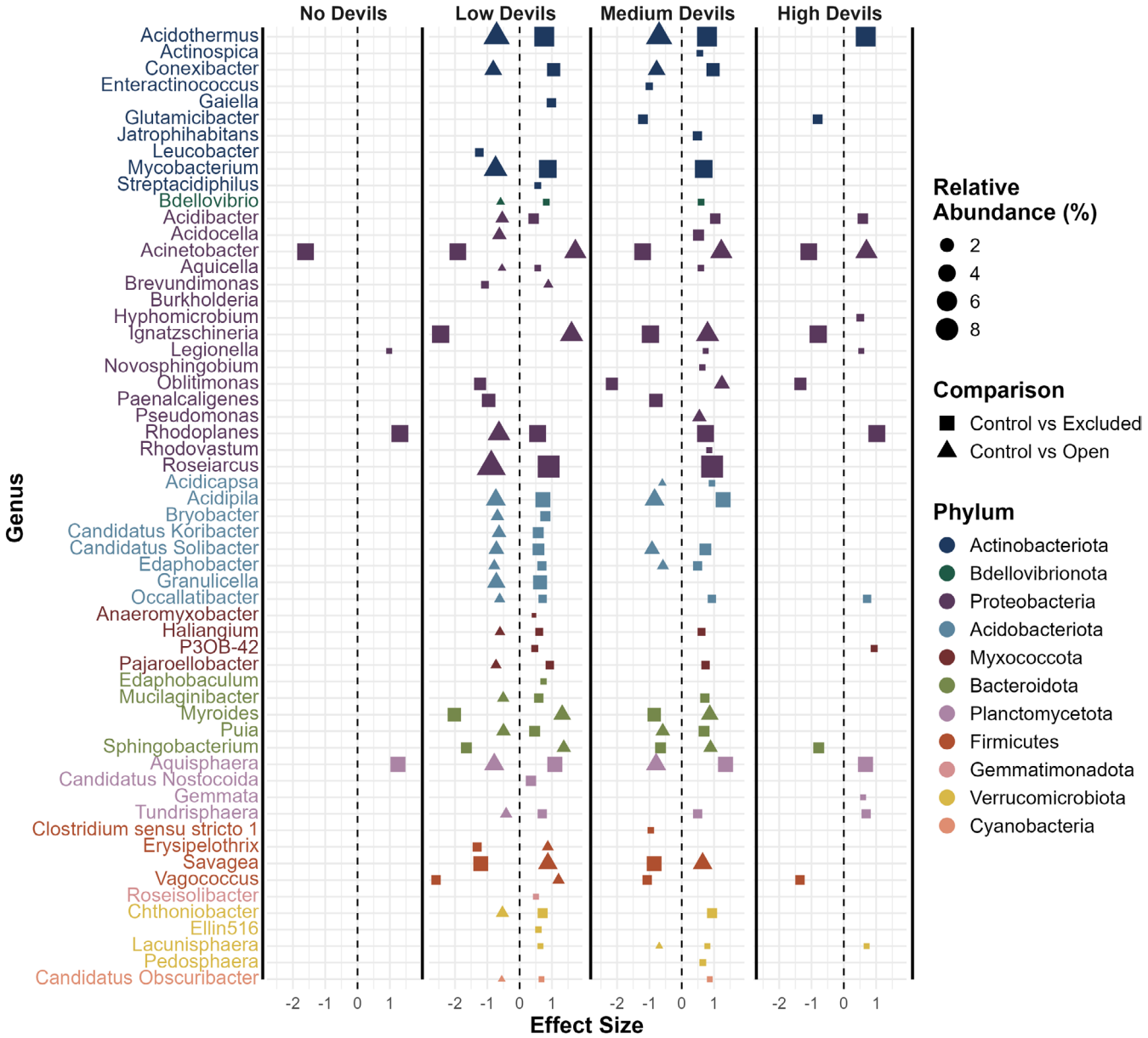

FIGURE 3 | Across all sites, 58 bacterial genera were identified as differentially abundant between treatments (based on ALDEx2 analysis for Days 5–15). Within each site (separated by solid vertical lines), symbol shape indicates the treatment comparison, symbol size represents the relative abundance of each genus, and symbol color indicates the phylum to which each genus belongs. Positive effect sizes correspond to genera that were more abundant at carcass than control locations, and negative effect sizes correspond to genera that were more abundant at control than carcass locations.

Changes in soil nutrient dynamics between summer and winter (Figure S2) were reflected in bacterial community composition (Figure S8). Fungal ($\chi^2 = 23.7$, $p < 0.001$) and bacterial ($\chi^2 = 46.8$, $p < 0.001$) α-diversity were higher in summer than in winter across all sites, and the relative abundance of fungi exhibiting all three trophic modes was higher in summer than in winter ($\chi^2 = 5.0$; $p < 0.05$). We also observed an interaction between season and location for "saprotroph-symbiotroph" fungi, which were more abundant at carcasses than at controls in the summer but not in winter ($\chi^2 = 11.3$; $p < 0.01$). Bacterial α-diversity was lower under carcasses, though not significantly different between excluded and open carcasses. Bacterial β-diversity differed between season and site ($F_{3,137} = 3.80$, $p < 0.05$) and under carcasses relative to paired controls ($F_{3,137} = 32.2$; $p < 0.001$). Overall, 176 (63%) microbial families were present in both seasons; of these, 91 (34%) were detected only in summer and 11 (6%) were detected only in winter.

4 | Discussion

Disease-induced declines in Tasmanian devil populations dramatically altered the activity of subordinate scavengers and the availability of nutrients for plant and microbial assimilation. Here, we reveal how apex scavengers mediate belowground processes by altering the function of carrion food webs. Specifically, carcass-derived nutrient fluxes to soil were significantly greater at sites with low devil densities and under

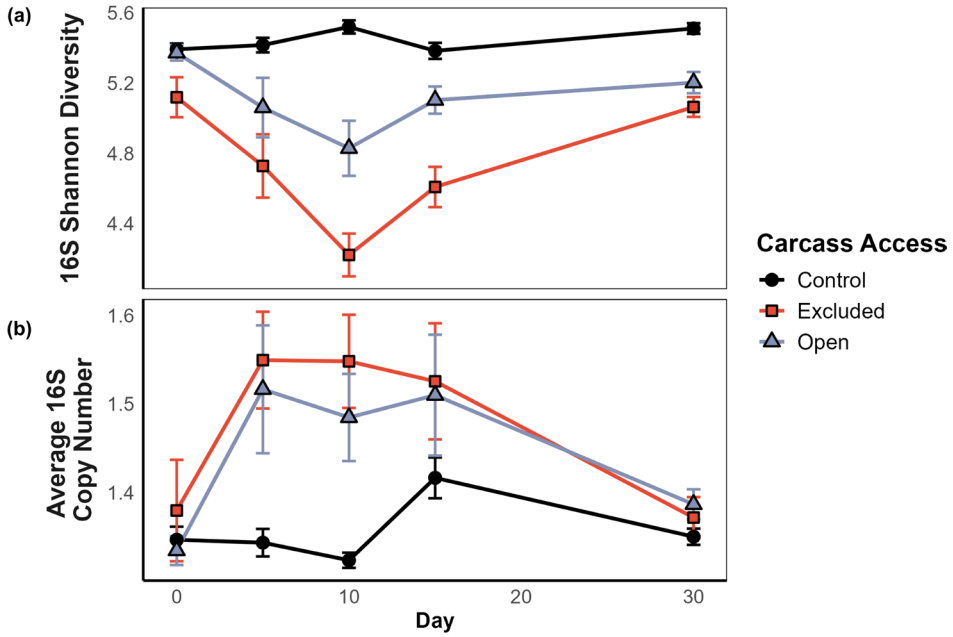

FIGURE 4 | Soil bacterial a-diversity (Shannon) and 16S copy number under carcasses and at control locations, averaged across sites. Carcass presence increased (a) average 16S copy number and (b) decreased 16S Shannon diversity compared to paired controls. Average 16S copy number under carcasses (excluded and open) was significantly higher than paired controls from Days 5 to 15, and 16S Shannon diversity was higher at controls than carcasses (excluded and open) from Days 5 to 30. Significance is defined as $p < 0.05$ for all panels; standard error bars reflect variability across sites and replicates ($n = 24$).

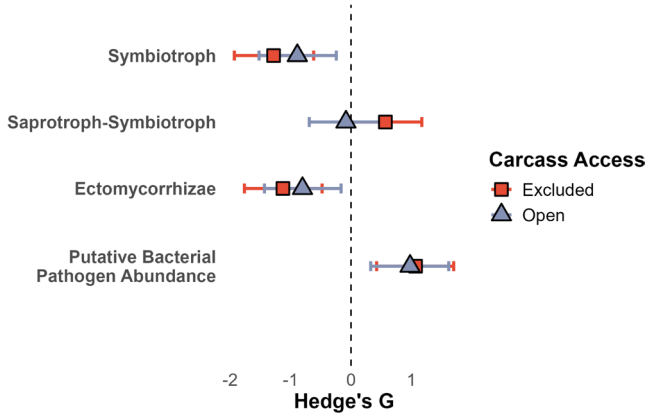

FIGURE 5 | Effect plot showing Hedge's *G*, a measure used to quantify effect sizes between two group means (here, carcass vs. paired controls) during the summer trial for fungal groups (at Day 30) and putative bacterial pathogens (at Day 15), across all sites. Regardless of access, carcass presence decreased the relative abundance of fungal symbiotrophs while increasing the relative abundance of fungal saprotroph-symbiotrophs and putative bacterial pathogens. Points with error bars that do not cross zero (dashed line) indicate significant differences from controls. Significance is defined as $p < 0.05$ for all panels; standard error bars reflect variability across sites and replicates ($n = 24$).

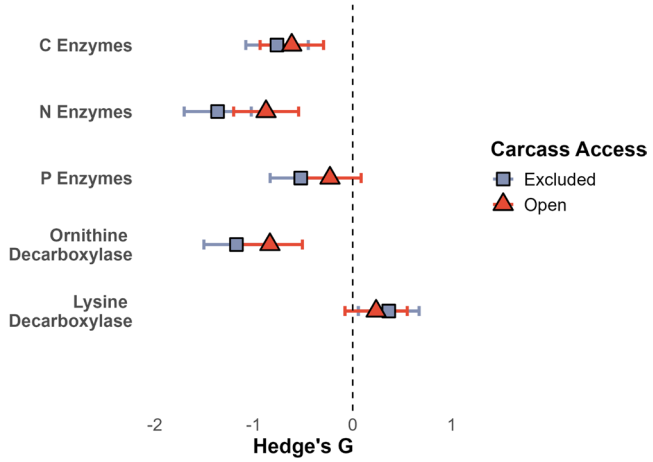

FIGURE 6 | Effect plot showing Hedge's *G*, a measure used to quantify effect sizes between two group means (here, carcass vs. paired controls) during the summer trial for various enzyme-encoding genes, averaged across sites and times after carcass placement. Carcass presence reduced the relative abundance of all enzyme groups except for lysine decarboxylase as compared to control locations. Points with error bars that do not cross zero (dashed line) indicate significant differences from controls. Significance is defined as $p < 0.05$ for all panels; standard error bars reflect variability across sites and replicates ($n = 24$).

carcasses where adult devils were excluded. These nutrients favored copiotrophic bacteria and putative pathogens, while reducing symbiotrophic fungi and the saprotrophic functions of microbes that convert organic nutrients into bioavailable forms. Soil biogeochemical responses to devils were modified by seasonality, with colder and wetter winter conditions reducing rates of carcass discovery and consumption, the activity of invertebrate and microbial consumers, and the flux of carcass-derived nutrients belowground. Our findings illustrate how apex scavenger declines can have cascading impacts on ecological populations and communities with broad implications for nutrient cycling, microbial activity, and soil carbon storage and persistence (Bartel et al. 2024; Stephenson et al. 2024).

Carcass consumption rates, which indirectly affected ecosystem properties, were strongly influenced by devil density, access, and population demographics. Game camera photos confirmed small juvenile devils were abundant at the high devil site during the summer and often breached exclusion cages, causing overall carcass consumption to be similar across devil access treatments. These cage breaches also demonstrated that juvenile devils and other subordinate scavengers, including quolls, possums, rats, and birds, were not functionally equivalent to adult devils (Bartel et al. 2025; Jones et al. 2008). Specifically, a greater influx of carcass-derived nutrients to the soil occurred when adult devils were excluded or present at low densities, revealing clear functional differences between apex and subordinate scavenger guilds. Previous work also suggests the diet composition of juvenile and adult devils is distinct, with juveniles relying more heavily on small mammals, birds, and invertebrates than adult devils, which typically consume larger mammals, such as pademelons (Bell et al. 2020; Jones and Barmuta 2000).

Although subordinate scavengers rarely consumed all soft tissues, they often ruptured hides, facilitating carcass colonization by invertebrates such as flies and beetles. In addition to the direct effects of invertebrate consumption on carcass decomposition, invertebrates can shape the carcass microbiome by introducing novel microorganisms that further accelerate carcass bloat, rupture, and tissue solubilization (Burcham et al. 2024). Although the mass dispersal of invertebrates can scatter carcass-derived nutrients across the landscape (Lashley et al. 2018), decomposition islands are generally smaller than those created by vertebrate scavengers (Aitkenhead-Peterson et al. 2012), resulting in spatially constrained nutrient hotspots that subsidize soil microbiomes (Keenan et al. 2018; Parmenter and MacMahon 2009). Specifically, we found that soils under carcasses were associated with lower microbial community α-diversity, higher 16S rRNA operon copy numbers (Roller et al. 2016), and faster-growing copiotrophic phyla (i.e., Firmicutes, Bacteroidota, and Proteobacteriota; Fierer et al. 2007). Yet, these effects were seasonal; given that invertebrates were mostly inactive in the winter months and juvenile devils were primarily detected in the summer, multiyear dynamics could be revealing.

The classical growth rate versus yield tradeoff predicts that high-resource environments favor faster-growing, competitive taxa with higher energetic costs (e.g., via more transporters, enzymes, and overflow metabolism) while nutrient-poor conditions favor slower-growing, but more efficient taxa (Wortel et al. 2018). When bioavailable nutrients are scarce, active taxa can divert energy toward the production of extracellular enzymes that depolymerize complex organic matter into bioavailable forms (Allison and Vitousek 2005). Using PICRUSt2, we found that the influx of easily assimilable, carcass-derived nutrients to soils reduced the predicted abundance of a gene typically associated with animal protein depolymerization—ornithine decarboxylase, which converts ornithine to the diamine putrescine—and genes coding for seven hydrolytic enzymes associated with the soil biogeochemical cycling of carbon, nitrogen, and phosphorus (Table S15). Ornithine decarboxylase genes were previously found to be elevated within human cadavers and mouse carcasses (Metcalf et al. 2016), suggesting endogenous microbial communities catalyzed tissue decomposition during the bloat stage. We suspect the products of enzyme hydrolysis are then released belowground during the carcass rupture and seepage stage, where they can be directly assimilated by opportunistic soil taxa (Ramin and Allison 2019), thereby reducing the relative abundance of enzyme pathways expressed at the community level. Although reference genomes are better characterized for environments, such as the human gut than for soils, recent benchmarking suggests PICRUSt2 can generate useful approximations of metabolic potential in ecological datasets (Douglas et al. 2020). Here, we found that predicted pathways aligned well with biogeochemical measurements, suggesting PICRUSt2 outputs captured functional shifts in processes that influenced microbial metabolic efficiency; these predictions would be further strengthened by targeted validation (e.g., polyamine metabolomics or enzyme activity assays). Regardless, while the short-term impacts of carcass-derived nutrients on the soil microbiome are clear, the longer-term biogeochemical consequences are not (Barnett et al. 2021).

Long-term studies across multiple seasons are required to disentangle whether proximate changes in interkingdom feedbacks and microbial traits will alter soil carbon trajectories, which can take decades to manifest (Schmidt et al. 2011). For instance, copiotrophs exhibit rapid but inefficient growth, with potentially counteracting effects on soil carbon storage. On one hand, rapid growth produces large pools of microbial necromass that can associate with soil minerals to increase soil organic carbon formation and sequestration (Malik et al. 2020). On the other hand, rapid growth is often associated with lower carbon use efficiency (i.e., more carbon dioxide released per unit of biomass produced), which can increase soil carbon loss to the atmosphere (Tao et al. 2023). Previous research has shown that carcass inputs have persistent effects on soil chemistry, microbiomes, and plant community composition, increasing landscape heterogeneity and ecosystem productivity (Barton et al. 2016; Ferraro et al. 2024). Biogeochemical modeling of this study system also suggests high-quality devil scat inputs enhance carbon storage in microbial biomass, increase above and belowground net primary productivity, and buffer against declines in soil carbon stocks under future climate conditions (Stephenson et al. 2024). The contrasting effects of microbial life history traits on soil carbon cycling underscore the need for deeper investigation, particularly in carbon-dense Tasmanian forest ecosystems that are susceptible to biodiversity loss and shifting climate and resource regimes (Stephenson et al. 2024).

Our study highlights the ability of apex scavengers to shape ecological functions performed by soil microbiomes, offering a clear example of an interkingdom feedback to be considered in ecological disturbance frameworks (Stephenson et al. 2024). Notably, our results suggest adult devils amplify the spatial distribution of carcass-derived nutrients relative to smaller subordinate scavengers via rapid carcass removal and waste excretion, thereby multiplying the occurrence of relatively smaller nutrient "hot spots" and "hot moments" across the landscape (DeBruyn et al. 2024; Stephenson et al. 2024). These effects are amplified in the winter when the activity of competing scavengers, like ectothermic invertebrates and microorganisms, is reduced. Rapid carcass removal by devils may provide an additional ecosystem service by reducing pathogen loads (and potentially the spread of zoonotic disease; Nieder et al. 2018), a function previously noted for vultures, which can reduce anthrax spillover events

by digesting metabolically active bacteria before they sporulate (Den Heever et al. 2021). By highlighting the critical role apex scavengers play in maintaining ecosystem function and soil carbon sequestration (Stephenson et al. 2024), we suggest zoogeochemical feedbacks should be considered in ecosystem models (Schmitz et al. 2018).

Author Contributions

Torrey Stephenson: data curation, formal analysis, investigation, visualization, writing – original draft, writing – review and editing. **David W. Crowder:** conceptualization, funding acquisition, writing – review and editing. **Ernest Osburn:** investigation, methodology, supervision, writing – review and editing. **Michael Strickland:** conceptualization, funding acquisition, supervision, writing – review and editing. **Menna Jones:** conceptualization, funding acquisition, methodology, project administration, resources, supervision, writing – review and editing. **Savannah Bartel:** investigation, methodology, writing – review and editing. **Kawinwit Kittipalawattanapol:** investigation, writing – review and editing. **Calum X. Cunningham:** conceptualization, funding acquisition, writing – review and editing. **Tara Hudiburg:** conceptualization, funding acquisition, supervision, writing – review and editing. **Andrew Storfer:** conceptualization, funding acquisition, writing – review and editing. **Julia Piaskowski:** formal analysis, methodology, writing – review and editing. **Laurel Lynch:** conceptualization, formal analysis, funding acquisition, investigation, methodology, project administration, supervision, writing – review and editing.

Acknowledgments

The authors would like to acknowledge the invaluable contributions of David Green, Justin Mathias, Cooper Moon, and Vince Scoleri to this research. This material is based upon work supported by the National Science Foundation under Award DEB-2054716. Any opinions, findings, and conclusions or recommendations expressed in this material are those of the author(s) and do not necessarily reflect the views of the National Science Foundation. Soil and foliar samples were collected in accordance with the Tasmania Department of Natural Resources and Environment permit ES-22276 and handled following the US Department of Agriculture quarantine permit P526P-21-06775. This project was approved by the University of Tasmania Animal Ethics Committee (Project #27172); all team members completed the appropriate Animal Ethics Training. We acknowledge this research was conducted in lutruwita/Tasmania on the unceded lands of the nuenonne (Bruny Island), noeteeler (West Takone), manegin (Salmon River), and kunnarra kuna (Blue Tier region) peoples.

Conflicts of Interest

The authors declare no conflicts of interest.

Data Availability Statement

All data (biogeochemical, microbial relative abundance summaries, pathogen information) and code used in the study are available via Zenodo at https://doi.org/10.5281/zenodo.17101314. Raw sequences are deposited in the NCBI archive under accession number PRJNA1238269.

References

Abarenkov, K., R. Henrik Nilsson, K. Larsson, et al. 2010. "The UNITE Database for Molecular Identification of Fungi–Recent Updates and Future Perspectives." *New Phytologist* 186, no. 2: 281–285.

Aitkenhead-Peterson, J. A., C. G. Owings, M. B. Alexander, N. Larison, and J. A. Bytheway. 2012. "Mapping the Lateral Extent of Human Cadaver Decomposition With Soil Chemistry." *Forensic Science International* 216, no. 1: 127–134. https://doi.org/10.1016/j.forsciint.2011.09.007.

Allison, S. D., and P. M. Vitousek. 2005. "Responses of Extracellular Enzymes to Simple and Complex Nutrient Inputs." *Soil Biology and Biochemistry* 37, no. 5: 937–944. https://doi.org/10.1016/j.soilbio.2004.09.014.

Altschul, S. F., W. Gish, W. Miller, E. W. Myers, and D. J. Lipman. 1990. "Basic Local Alignment Search Tool." *Journal of Molecular Biology* 215, no. 3: 403–410. https://doi.org/10.1016/S0022-2836(05)80360-2.

Andersen, G. E., C. N. Johnson, L. A. Barmuta, and M. E. Jones. 2017. "Dietary Partitioning of Australia's Two Marsupial Hypercarnivores, the Tasmanian Devil and the Spotted-Tailed Quoll, Across Their Shared Distributional Range." *PLoS One* 12, no. 11: e0188529. https://doi.org/10.1371/journal.pone.0188529.

Barnett, S. E., N. D. Youngblut, C. N. Koechli, and D. H. Buckley. 2021. "Life History Strategies Explain Bacterial Activity in the Soil Carbon Cycle (2021.03.19.436178)." *BioRxiv*. https://doi.org/10.1101/2021.03.19.436178.

Bar-On, Y. M., R. Phillips, and R. Milo. 2018. "The Biomass Distribution on Earth." *Proceedings of the National Academy of Sciences* 115, no. 25: 6506–6511. https://doi.org/10.1073/pnas.1711842115.

Bartel, S. L., L. M. Lynch, T. Stephenson, M. E. Jones, M. S. Strickland, and A. Storfer. 2025. "Decline of an Apex Vertebrate Scavenger Increases Carrion Use by Invertebrates." *Ecology*. https://doi.org/10.1002/ecy.70214.

Bartel, S. L., T. Stephenson, D. W. Crowder, et al. 2024. "Global Change Influences Scavenging and Carrion Decomposition." *Trends in Ecology & Evolution* 39, no. 2: 152–164. https://doi.org/10.1016/j.tree.2023.09.008.

Barton, P. S., S. McIntyre, M. J. Evans, J. K. Bump, S. A. Cunningham, and A. D. Manning. 2016. "Substantial Long-Term Effects of Carcass Addition on Soil and Plants in a Grassy Eucalypt Woodland." *Ecosphere* 7, no. 10: 1–11. https://doi.org/10.1002/ecs2.1537.

Bell, O., M. E. Jones, M. Ruiz-Aravena, R. K. Hamede, S. Bearhop, and R. A. McDonald. 2020. "Age-Related Variation in the Trophic Characteristics of a Marsupial Carnivore, the Tasmanian Devil *Sarcophilus harrisii*." *Ecology and Evolution* 10, no. 14: 7861–7871. https://doi.org/10.1002/ece3.6513.

Benbow, M. E., P. S. Barton, M. D. Ulyshen, et al. 2019. "Necrobiome Framework for Bridging Decomposition Ecology of Autotrophically and Heterotrophically Derived Organic Matter." *Ecological Monographs* 89, no. 1: 1–29. https://doi.org/10.1002/ecm.1331.

Burcham, Z. M., A. D. Belk, B. B. McGivern, et al. 2024. "A Conserved Interdomain Microbial Network Underpins Cadaver Decomposition Despite Environmental Variables." *Nature Microbiology* 9, no. 3: 595–613. https://doi.org/10.1038/s41564-023-01580-y.

Callahan, B. J., P. J. McMurdie, M. J. Rosen, A. W. Han, A. J. A. Johnson, and S. P. Holmes. 2016. "DADA2: High-Resolution Sample Inference From Illumina Amplicon Data." *Nature Methods* 13, no. 7: 581–583. https://doi.org/10.1038/nmeth.3869.

Carter, D. O., D. Yellowlees, and M. Tibbett. 2006. "Cadaver Decomposition in Terrestrial Ecosystems." *Naturwissenschaften* 94, no. 1: 12–24. https://doi.org/10.1007/s00114-006-0159-1.

Clement, D. T., D. G. Gallinson, R. K. Hamede, et al. 2025. "Coevolution Promotes the Coexistence of Tasmanian Devils and a Fatal, Transmissible Cancer." *Evolution* 79, no. 1: 100–118. https://doi.org/10.1093/evolut/qpae143.

Cunningham, C. X., S. Comte, H. McCallum, et al. 2021. "Quantifying 25 Years of Disease-Caused Declines in Tasmanian Devil Populations:

Host Density Drives Spatial Pathogen Spread." *Ecology Letters* 24, no. 5: 958–969. https://doi.org/10.1111/ele.13703.

Cunningham, C. X., C. N. Johnson, L. A. Barmuta, T. Hollings, E. J. Woehler, and M. E. Jones. 2018. "Top Carnivore Decline Has Cascading Effects on Scavengers and Carrion Persistence." *Proceedings of the Royal Society B: Biological Sciences* 285, no. 1892: 20181582. https://doi.org/10.1098/rspb.2018.1582.

DeBruyn, J. M., S. W. Keenan, and L. S. Taylor. 2024. "From Carrion to Soil: Microbial Recycling of Animal Carcasses." *Trends in Microbiology* 33, no. 2: 194–207. https://doi.org/10.1016/j.tim.2024.09.003.

Den Heever, L. V., L. J. Thompson, W. W. Bowerman, et al. 2021. "Reviewing the Role of Vultures at the Human-Wildlife-Livestock Disease Interface: An African Perspective." *Journal of Raptor Research* 55, no. 3: 311–327. https://doi.org/10.3356/JRR-20-22.

Doane, T. A., and W. R. Horwáth. 2003. "Spectrophotometric Determination of Nitrate With a Single Reagent." *Analytical Letters* 36, no. 12: 2713–2722. https://doi.org/10.1081/AL-120024647.

Douglas, G. M., V. J. Maffei, J. R. Zaneveld, et al. 2020. "PICRUSt2 for Prediction of Metagenome Functions." *Nature Biotechnology* 38, no. 6: 685–688. https://doi.org/10.1038/s41587-020-0548-6.

Epstein, B., M. Jones, R. Hamede, et al. 2016. "Rapid Evolutionary Response to a Transmissible Cancer in Tasmanian Devils." *Nature Communications* 7: 12684.

Estes, J. A., J. Terborgh, J. S. Brashares, et al. 2011. "Trophic Downgrading of Planet Earth." *Science* 333, no. 6040: 301–306.

Fancourt, B. A. 2015. "Making a Killing: Photographic Evidence of Predation of a Tasmanian Pademelon (*Thylogale billardierii*) by a Feral Cat (*Felis catus*)." *Australian Mammalogy* 37, no. 1: 120–124.

Ferraro, K. M., D. Albrecht, J. G. Hendrix, et al. 2024. "The Biogeochemical Boomerang: Site Fidelity Creates Nutritional Hotspots That May Promote Recurrent Calving Site Reuse." *Ecology Letters* 27, no. 8: e14491. https://doi.org/10.1111/ele.14491.

Fierer, N., M. A. Bradford, and R. B. Jackson. 2007. "Toward an Ecological Classification of Soil Bacteria." *Ecology* 88, no. 6: 1354–1364. https://doi.org/10.1890/05-1839.

Gloor, G. B., J. M. Macklaim, and A. D. Fernandes. 2016. "Displaying Variation in Large Datasets: Plotting a Visual Summary of Effect Sizes." *Journal of Computational and Graphical Statistics* 25, no. 3: 971–979. https://doi.org/10.1080/10618600.2015.1131161.

Gold, M., F. Von Allmen, C. Zurbrügg, J. Zhang, and A. Mathys. 2020. "Identification of Bacteria in Two Food Waste Black Soldier Fly Larvae Rearing Residues." *Frontiers in Microbiology* 11: 582867. https://doi.org/10.3389/fmicb.2020.582867.

Gupta, A. K., M. S. Dharne, A. Y. Rangrez, et al. 2011. "*Ignatzschineria indica* Sp. nov. and *Ignatzschineria ureiclastica* sp. nov., Isolated From Adult Flesh Flies (Diptera: Sarcophagidae)." *International Journal of Systematic and Evolutionary Microbiology* 61, no. 6: 1360–1369. https://doi.org/10.1099/ijs.0.018622-0.

Hartig, F. 2022. "DHARMa: Residual Diagnostics for Hierarchical (Multi-Level/Mixed) Regression Models." https://CRAN.R-project.org/package=DHARMa.

Hawkins, C. E., C. Baars, H. Hesterman, et al. 2006. "Emerging Disease and Population Decline of an Island Endemic, the Tasmanian Devil *Sarcophilus harrisii*." *Biological Conservation* 131, no. 2: 307–324. https://doi.org/10.1016/j.biocon.2006.04.010.

Jones, M. 1997. "Character Displacement in Australian Dasyurid Carnivores: Size Relationships and Prey Size Patterns." *Ecology* 78, no. 8: 2569–2587. https://doi.org/10.1890/0012-9658(1997)078%255B2569:CDIADC%255D2.0.CO;2.

Jones, M. E., and L. A. Barmuta. 2000. "Niche Differentiation Among Sympatric Australian Dasyurid Carnivores." *Journal of Mammalogy* 81, no. 2: 434–447. https://doi.org/10.1644/1545-1542(2000)081%253C0434:NDASAD%253E2.0.CO;2.

Jones, M. E., A. Cockburn, R. Hamede, et al. 2008. "Life-History Change in Disease-Ravaged Tasmanian Devil Populations." *Proceedings of the National Academy of Sciences of the United States of America* 105, no. 29: 10023–10027. https://doi.org/10.1073/pnas.0711236105.

Keenan, S. W., S. M. Schaeffer, V. L. Jin, and J. M. DeBruyn. 2018. "Mortality Hotspots: Nitrogen Cycling in Forest Soils During Vertebrate Decomposition." *Soil Biology and Biochemistry* 121: 165–176. https://doi.org/10.1016/j.soilbio.2018.03.005.

Krassowski, M., M. Arts, C. Lagger, and Max. 2022. "Krassowski/Complex-Upset: V1.3.5 (Version v1.3.5) [Computer Software]." *Zenodo*. https://doi.org/10.5281/zenodo.7314197.

Lashley, M. A., H. R. Jordan, J. K. Tomberlin, and B. T. Barton. 2018. "Indirect Effects of Larval Dispersal Following Mass Mortality Events." *Ecology* 99, no. 2: 491–493.

Lee, J. K., Y. Y. Lee, K. H. Park, et al. 2014. "*Wohlfahrtiimonas larvae* sp. nov., Isolated From the Larval Gut of *Hermetia Illucens* (Diptera: Stratiomyidae)." *Antonie Van Leeuwenhoek* 105, no. 1: 15–21. https://doi.org/10.1007/s10482-013-0048-5.

Lenth, R. V. 2024. "emmeans: Estimated Marginal Means, Aka Least-Squares Means." https://CRAN.R-project.org/package=emmeans.

Ma, S., W. Zhu, W. Wang, X. Li, and Z. Sheng. 2023. "Microbial Assemblies With Distinct Trophic Strategies Drive Changes in Soil Microbial Carbon Use Efficiency Along Vegetation Primary Succession in a Glacier Retreat Area of the Southeastern Tibetan Plateau." *Science of the Total Environment* 867: 161587. https://doi.org/10.1016/j.scitotenv.2023.161587.

Malik, A. A., J. B. H. Martiny, E. L. Brodie, A. C. Martiny, K. K. Treseder, and S. D. Allison. 2020. "Defining Trait-Based Microbial Strategies With Consequences for Soil Carbon Cycling Under Climate Change." *ISME Journal* 14, no. 1: 1–9. https://doi.org/10.1038/s41396-019-0510-0.

Margres, M. J., M. Ruiz-Aravena, R. Hamede, et al. 2020. "Spontaneous Tumor Regression in Tasmanian Devils Associated With RASL11A Activation." *Genetics* 215, no. 4: 1143–1152.

McMurdie, P. J., and S. Holmes. 2013. "phyloseq: An R Package for Reproducible Interactive Analysis and Graphics of Microbiome Census Data." *PLoS One* 8, no. 4: e61217. https://doi.org/10.1371/journal.pone.0061217.

Metcalf, J. L., Z. Z. Xu, S. Weiss, et al. 2016. "Microbial Community Assembly and Metabolic Function During Mammalian Corpse Decomposition." *Science* 351, no. 6269: 158–162.

Nguyen, N. H., Z. Song, S. T. Bates, et al. 2016. "FUNGuild: An Open Annotation Tool for Parsing Fungal Community Datasets by Ecological Guild." *Fungal Ecology* 20: 241–248. https://doi.org/10.1016/j.funeco.2015.06.006.

Nieder, R., D. K. Benbi, and F. X. Reichl. 2018. "Soil as a Transmitter of Human Pathogens." In *Soil Components and Human Health*, edited by R. Nieder, D. K. Benbi, and F. X. Reichl, 723–827. Springer Netherlands. https://doi.org/10.1007/978-94-024-1222-2_13.

Oksanen, J., G. L. Simpson, F. G. Blanchet, et al. 2001. "vegan: Community Ecology Package (p. 2.6-8) [Dataset]." https://doi.org/10.32614/CRAN.package.vegan.

Ordiz, A., M. Aronsson, J. Persson, O.-G. Støen, J. E. Swenson, and J. Kindberg. 2021. "Effects of Human Disturbance on Terrestrial Apex Predators." *Diversity* 13, no. 2: 68. https://doi.org/10.3390/d13020068.

Parmenter, R. R., and J. A. MacMahon. 2009. "Carrion Decomposition and Nutrient Cycling in a Semiarid Shrub–Steppe Ecosystem." *Ecological Monographs* 79, no. 4: 637–661. https://doi.org/10.1890/08-0972.1.

Pemberton, D. 1990. "Social Organisation and Behaviour of the Tasmanian Devil, *Sarcophilus harrisii* [Thesis, University of Tasmania]." https://doi.org/10.25959/23211758.v1.

Pemberton, D., S. Gales, B. Bauer, R. Gales, B. Lazenby, and K. Medlock. 2008. "The Diet of the Tasmanian Devil, *Sarcophilus harrisii*, as Determined From Analysis of Scat and Stomach Contents." *Papers and Proceedings of the Royal Society of Tasmania* 142, no. 2: 13–22.

Pemberton, D., and D. Renouf. 1993. "A Field-Study of Communication and Social-Behavior of the Tasmanian Devil at Feeding Sites." *Australian Journal of Zoology* 41, no. 5: 507–526.

Quast, C., E. Pruesse, P. Yilmaz, et al. 2013. "The SILVA Ribosomal RNA Gene Database Project: Improved Data Processing and Web-Based Tools." *Nucleic Acids Research* 41, no. D1: D590–D596. https://doi.org/10.1093/nar/gks1219.

R Core Team. 2024. *R: A Language and Environment for Statistical Computing*. R Foundation for Statistical Computing. https://www.R-project.org/.

Ramin, K. I., and S. D. Allison. 2019. "Bacterial Tradeoffs in Growth Rate and Extracellular Enzymes." *Frontiers in Microbiology* 10: 2956. https://doi.org/10.3389/fmicb.2019.02956.

Ripple, W. J., G. Chapron, J. V. López-Bao, et al. 2017. "Conserving the World's Megafauna and Biodiversity: The Fierce Urgency of Now." *Bioscience* 67, no. 3: 197–200.

Ripple, W. J., J. A. Estes, R. L. Beschta, et al. 2014. "Status and Ecological Effects of the World's Largest Carnivores." *Science* 343, no. 6167: 1241484.

Roller, B. R. K., S. F. Stoddard, and T. M. Schmidt. 2016. "Exploiting rRNA Operon Copy Number to Investigate Bacterial Reproductive Strategies." *Nature Microbiology* 1: 16160. https://doi.org/10.1038/nmicrobiol.2016.160.

Schmidt, M. W. I., M. S. Torn, S. Abiven, et al. 2011. "Persistence of Soil Organic Matter as an Ecosystem Property." *Nature* 478, no. 7367: 49–56. https://doi.org/10.1038/nature10386.

Schmitz, O. J., C. C. Wilmers, S. J. Leroux, et al. 2018. "Animals and the Zoogeochemistry of the Carbon Cycle." *Science* 362, no. 6419: eaar3213. https://doi.org/10.1126/science.aar3213.

Stephenson, T., T. Hudiburg, J. M. Mathias, M. Jones, and L. M. Lynch. 2024. "Do Tasmanian Devil Declines Impact Ecosystem Function?" *Global Change Biology* 30, no. 7: e17413. https://doi.org/10.1111/gcb.17413.

Sterner, R. W., and J. J. Elser. 2002. *Ecological Stoichiometry: The Biology of Elements From Molecules to the Biosphere*. Princeton university press.

Strickland, M. S., A. D. Keiser, and M. A. Bradford. 2015. "Climate History Shapes Contemporary Leaf Litter Decomposition." *Biogeochemistry* 122, no. 2–3: 165–174. https://doi.org/10.1007/s10533-014-0065-0.

Tao, F., Y. Huang, B. A. Hungate, et al. 2023. "Microbial Carbon Use Efficiency Promotes Global Soil Carbon Storage." *Nature* 618: 1–5. https://doi.org/10.1038/s41586-023-06042-3.

Vogel, H., S. P. Shukla, T. Engl, et al. 2017. "The Digestive and Defensive Basis of Carcass Utilization by the Burying Beetle and Its Microbiota." *Nature Communications* 8, no. 1: 15186. https://doi.org/10.1038/ncomms15186.

Walters, W., E. R. Hyde, D. Berg-Lyons, et al. 2016. "Improved Bacterial 16S rRNA Gene (V4 and V4-5) and Fungal Internal Transcribed Spacer Marker Gene Primers for Microbial Community Surveys." *mSystems* 1, no. 1: e00009-15. https://doi.org/10.1128/mSystems.00009-15.

Weatherburn, M. W. 1967. "Phenol-Hypochlorite Reaction for Determination of Ammonia." *Analytical Chemistry* 39, no. 8: 971–974. https://doi.org/10.1021/ac60252a045.

White, T. J., T. D. Bruns, S. B. Lee, and J. W. Taylor. 1990. "Amplification and Direct Sequencing of Fungal Ribosomal RNA Genes for Phylogenetics." In *PCR Protocols: A Guide to Methods and Applications*, edited by M. A. Innis, D. H. Gelfand, J. J. Sninsky, and T. J. White, 315–322. Academic Press.

Woods, G. M., S. Fox, A. S. Flies, et al. 2018. "Two Decades of the Impact of Tasmanian Devil Facial Tumor Disease." *Integrative and Comparative Biology* 58, no. 6: 1043–1054. https://doi.org/10.1093/icb/icy118.

Wortel, M. T., E. Noor, M. Ferris, F. J. Bruggeman, and W. Liebermeister. 2018. "Metabolic Enzyme Cost Explains Variable Trade-Offs Between Microbial Growth Rate and Yield." *PLoS Computational Biology* 14, no. 2: e1006010. https://doi.org/10.1371/journal.pcbi.1006010.

Wright, E. S. 2016. "Using DECIPHER v2.0 to Analyze Big Biological Sequence Data in R." *R Journal* 8, no. 1: 352. https://doi.org/10.32614/RJ-2016-025.

Yang, X., G. Jiang, Y. Zhang, et al. 2023. "MBPD: A Multiple Bacterial Pathogen Detection Pipeline for One Health Practices." *iMeta* 2, no. 1: e82. https://doi.org/10.1002/imt2.82.

Supporting Information

Additional supporting information can be found online in the Supporting Information section. **Data S1:** gcb70520-sup-0001-Supinfo.pdf.